

1 **Estimation of bubbled-mediated air/sea gas exchange from**
2 **concurrent DMS and CO₂ transfer velocities at intermediate-**
3 **high wind speeds**

4
5 **Thomas G. Bell^{1*}, Sebastian Landwehr², Scott D. Miller³, Warren J. de Bruyn⁴,**
6 **Adrian H. Callaghan^{5,6}, Brian Scanlon², Brian Ward², Mingxi Yang¹ and Eric S.**
7 **Saltzman⁷**

8 [1] Plymouth Marine Laboratory, Prospect Place, The Hoe, Plymouth, PL1 3DH, UK

9 [2] School of Physics, National University of Ireland, Galway, Ireland

10 [3] Atmospheric Sciences Research Center, State University of New York at Albany, NY, USA

11 [4] Schmid College of Science and Technology, Chapman University, Orange, California, CA, USA

12 [5] Scripps Institution of Oceanography, University of California San Diego, 9500 Gilman Drive, La
13 Jolla, CA 92093

14 [6] Now at: Department of Civil and Environmental Engineering, Imperial College London, South
15 Kensington Campus, London, SW7 2AZ, UK

16 [7] Department of Earth System Science, University of California, Irvine, CA, USA

17 *Correspondence to: T.G. Bell (tbe@pml.ac.uk)

18 **Abstract**

19 Simultaneous air/sea fluxes and concentration differences of dimethylsulfide (DMS) and
20 carbon dioxide (CO₂) were measured during a summertime North Atlantic cruise in 2011. This
21 dataset reveals significant differences between the gas transfer velocities of these two gases
22 (Δk_w) over a range of wind speeds up to 21 m s⁻¹. These differences occur at and above the
23 approximate wind speed threshold when waves begin breaking. Whitecap fraction (a proxy for
24 bubbles) was also measured and has a positive relationship with Δk_w , consistent with enhanced
25 bubble-mediated transfer of the less soluble CO₂ relative to that of the more soluble DMS.
26 However, the correlation of Δk_w with whitecap fraction is no stronger than with wind speed.
27 Models used to estimate bubble-mediated transfer from *in situ* whitecap fraction under-predict

28 the observations, particularly at intermediate wind speeds. Examining the differences between
29 gas transfer velocities of gases with different solubilities is a useful way to detect the impact
30 of bubble-mediated exchange. More simultaneous gas transfer measurements of different
31 solubility gases across a wide range of oceanic conditions are needed to understand the factors
32 controlling the magnitude and scaling of bubble-mediated gas exchange.

33 **1 Introduction**

34 Air/sea exchange is a significant process for many compounds that have biogeochemical and
35 climatic importance. Approximately 25% of the carbon dioxide (CO₂) released into the
36 atmosphere by anthropogenic activities has been taken up by the world oceans, which has
37 tempered its climate forcing while leading to ocean acidification (Le Quéré et al., 2015). The
38 biogenic gas dimethylsulfide (DMS) is a major contributor to the mass of marine atmospheric
39 aerosol (Virkkula et al., 2006). Volatile organic compounds (VOCs) such as isoprene, acetone
40 and acetaldehyde alter the oxidising capacity of the troposphere (Carpenter et al., 2012). The
41 solubility differences between these VOCs mean that their exchange is controlled to differing
42 degrees by processes on the water and air side of the air/sea interface (Yang et al., 2014). Many
43 of the factors influencing air/sea gas exchange will be altered by future changes in climate,
44 ocean circulation and biology. Earth system models and air quality models require more
45 accurate understanding of the processes that influence air/sea gas transfer.

46 Air/sea gas exchange is typically parameterised as a function of the ocean/atmosphere bulk
47 concentration difference (ΔC) and the physical mixing induced by wind stress at the interface
48 (Liss and Slater, 1974). The air/sea flux is typically described using the expression:

$$49 \quad \text{Flux} = K(C_w - \alpha C_a) \quad \text{Equation 1}$$

50 where C_w and C_a are the trace gas bulk concentration on either side of the interface, α is the
51 dimensionless water/air solubility of the gas in seawater and K is the gas transfer velocity. The
52 physics of gas transfer are implicitly represented by the gas transfer velocity, which is
53 commonly expressed in water-side units of velocity (cm hr⁻¹) and parameterized as a function
54 of wind speed (U_{10}) and Schmidt number (Sc). The simplicity of Equation 1 belies the
55 complexity of the processes involved in air/sea gas transfer. These processes include diffusion,
56 surface renewal and bubble-mediated transport. In turn, turbulence can be generated by wind
57 stress, wave-induced mixing, buoyancy, currents and wave breaking. A variety of theoretical,

58 laboratory, and field approaches have been used to study the processes that control air/sea
59 transfer, but we do not yet have a firm understanding of their relative importance under a range
60 of atmospheric and oceanic conditions.

61 The gas transfer-wind speed relationships for gases of different solubility may be affected by
62 breaking waves and bubbles (Keeling, 1993; Woolf, 1993, 1997). Gas invasion and evasion
63 via bubbles (k_{bub}) is sensitive to the void fraction (ratio of air volume to total volume) of the
64 bubble plume as well as the bubble size distribution. Bubble injection depth and cleanliness of
65 the surface (influenced by surfactants) affect bubble rise velocity and residence time. Bubble
66 residence time determines the time available for equilibration to occur while bubble volume,
67 pressure and gas diffusivity (Sc) govern the time needed for a bubble to equilibrate. The
68 magnitude of k_{bub} is expected to be greater for sparingly soluble gases (e.g. CO₂, dimensionless
69 solubility ~ 1) than for more soluble gases such as DMS (dimensionless solubility ~ 15),
70 particularly when bubbles are fully equilibrated. Bubble-mediated gas transfer has been
71 studied in the laboratory (Asher et al., 1996; Rhee et al., 2007) and using models (e.g. Woolf,
72 2005; Woolf et al., 2007; Fairall et al., 2011; Goddijn-Murphy et al., 2016).

73 Deliberate, dual-tracer techniques have estimated gas transfer by measuring the evasion of a
74 pair of sparingly soluble gases with different diffusivity (³He and SF₆, dimensionless solubility
75 ≤ 0.01). These studies observed a non-linear wind speed dependence of the gas transfer velocity,
76 in qualitative agreement with earlier studies in wind-wave tanks (e.g. Wanninkhof et al., 1985;
77 Liss and Merlivat, 1986; Watson et al., 1991). Direct, shipboard measurements of waterside
78 gas transfer have also been made by eddy covariance (e.g. McGillis et al., 2001; Huebert et al.,
79 2004; Marandino et al., 2007; Miller et al., 2010; Bell et al., 2013). These measurements
80 typically show DMS gas transfer velocities that are lower and exhibit more linear wind speed
81 dependence than the CO₂ transfer velocity-wind speed relationship inferred from dual tracer
82 studies (e.g. Yang et al., 2011; Goddijn-Murphy et al., 2012; Bell et al., 2015). It has been
83 suggested that the difference between the open ocean gas transfer velocities of CO₂ and DMS
84 is due to the reduced importance of bubble-mediated exchange for DMS (Blomquist et al.,
85 2006; Fairall et al., 2011; Goddijn-Murphy et al., 2016).

86 Only one set of concurrent CO₂ and DMS gas transfer velocity measurements have been
87 published to date (Miller et al., 2009). In that study, no data were collected for winds greater
88 than 10 m s⁻¹ and no statistically significant difference was observed in the CO₂ and DMS gas

89 transfer-wind speed relationships after normalising both gases to a common diffusivity. This
90 study presents a more extensive set of CO₂ and DMS gas transfer velocities that were measured
91 simultaneously aboard the R/V Knorr in the 2011 summertime North Atlantic in both
92 oligotrophic and highly productive waters. The DMS gas transfer velocities are discussed
93 separately in detail by Bell et al. (2013). Here we focus specifically on what can be learned
94 about gas transfer from the differences in behaviour of two different solubility gases at
95 intermediate and high wind speeds.

96 **2 Methods**

97 **2.1 Seawater, atmospheric and flux measurement systems**

98 The measurement setups for DMS and CO₂ concentrations in air and water and the eddy
99 covariance flux systems have been discussed in detail elsewhere (Miller et al., 2008; Saltzman
100 et al., 2009; Miller et al., 2010; Bell et al., 2013; Landwehr et al., 2014; Bell et al., 2015;
101 Landwehr et al., 2015). We provide a summary plus some additional details in the Appendix.

102 **2.2 Gas transfer velocity calculations**

103 In this section we describe the calculation of DMS and CO₂ gas transfer velocities from the
104 Knorr_11 cruise data. Measured gas transfer velocities are transformed into water side only
105 gas transfer velocities in order to remove the influence of air-side resistance. The relative
106 contribution of air-side resistance to the total resistance is a function of solubility and thus
107 different for the two gases. Finally, we discuss the most appropriate approach for comparing
108 the water-side gas transfer velocities, given that the two gases have different molecular
109 diffusivity and solubility.

110 Total gas transfer velocities (K) are calculated for CO₂ and DMS for each 10-minute flux
111 interval of the Knorr_11 cruise using Equation 1. The temperature-dependent dimensionless
112 solubilities of CO₂ and DMS in seawater are calculated following Weiss (1974) and Dacey et
113 al. (1984) respectively. These gas transfer velocities reflect the result of resistance on both sides
114 of the interface (Liss and Slater, 1974). The water side contribution to the total resistance is
115 determined as follows:

$$116 \quad k_w = \left[\frac{1}{K} - \frac{\alpha}{k_a} \right]^{-1} \quad \text{Equation 2}$$

117 where k_w and k_a are the air side and water side gas transfer velocities and α is dimensionless
 118 water/air solubility. Note that we use the α reported by Dacey et al. (1984) in these calculations
 119 rather than H as there appears to be an error in conversion between α and H in that study (see
 120 Supplemental information for discussion). CO_2 solubility is sufficiently low that air side
 121 resistance is negligible and the water side gas transfer is assumed equal to the total transfer
 122 velocity ($k_{\text{CO}_2} = K_{\text{CO}_2}$). The air side resistance for DMS needs to be accounted for because it is
 123 a moderately soluble gas (McGillis et al., 2000). Air side gas transfer velocities (k_a) for DMS
 124 were calculated for each 10 minute flux interval with the NOAA COAREG 3.1 model, using
 125 sea surface temperature (SST) and horizontal wind speed measured during the cruise. The
 126 NOAA COAREG 3.1 model (Fairall et al., 2011) is an extension of the COARE bulk
 127 parameterization for air/sea energy and momentum fluxes to simulate gas transfer (Fairall et
 128 al., 1998; Fairall et al., 2000). The air side resistance contributes about 5% on average to the
 129 total resistance for DMS. NOAA COAREG 3.1 model calculations were carried out using a
 130 turbulent/molecular coefficient, $A = 1.6$, and bubble-mediated coefficient, $B = 1.8$ (Fairall et
 131 al., 2011). Knorr_11 measurements of SST, air temperature, relative humidity, air pressure,
 132 downward radiation and wind speed were used as input parameters to the model. Note that the
 133 use of the COAREG 3.1 model introduces a small uncertainty in our estimates of waterside
 134 DMS gas transfer velocity (approximately $\pm 2\%$ when wind speed = 20 m s^{-1}).

135 To facilitate comparison of transfer coefficients for the two gases across a range of sea surface
 136 temperatures, gas transfer velocities are corrected for changes in molecular diffusivity and
 137 viscosity. The correction typically involves the normalisation of water side gas transfer
 138 velocities to a common Schmidt number ($Sc=660$), equivalent to CO_2 in seawater at 20°C :

$$139 \quad k_{x,660} = k_x \cdot \left(\frac{660}{Sc_x} \right)^{-0.5} \quad \text{Equation 3}$$

140 where subscript x refers to CO_2 or DMS (i.e. $k_{\text{DMS},660}$ and $k_{\text{CO}_2,660}$). Temperature-dependent
 141 Sc_{CO_2} and Sc_{DMS} were obtained using the *in situ* seawater temperature from the ship's bow
 142 sensor and parameterisations from Wanninkhof (1992) and Saltzman et al. (1993).

143 The Sc number normalization (Equation 3) is commonly used across the whole range of wind
 144 speeds. In fact, it is only appropriate at low or moderate winds when interfacial gas transfer
 145 dominates over bubble-mediated gas exchange. If bubbles are an important component of gas

146 transfer then solubility also plays a role and normalization based on Sc alone may not be
147 sufficient.

148 To develop a more rigorous comparison of k_{DMS} and k_{CO_2} , we normalized the water side
149 transfer velocities of DMS to the Schmidt number of CO_2 at the *in situ* sea surface temperature
150 of each 10-minute flux interval, as follows:

$$151 \quad k_{DMS,Sc} = k_{DMS} \left(\frac{Sc_{CO_2}}{Sc_{DMS}} \right)^{-0.5} \quad \text{Equation 4}$$

152 where Sc_{CO_2} and Sc_{DMS} are the Schmidt numbers of CO_2 and DMS at the *in situ* sea surface
153 temperature. Compared to normalizing both DMS and CO_2 to $Sc=660$, this approach has the
154 advantage of correcting only k_{DMS} , with no correction to k_{CO_2} . The Sc correction for DMS
155 should be reasonably accurate, assuming that the bubble-mediated transfer for the more soluble
156 DMS is relatively small.

157 On the Knorr_11 cruise, the variability in sea surface temperature was small ($1\sigma = \pm 1^\circ C$). As
158 a result, there is little difference in the variability or wind speed dependence of Sc -corrected
159 k_{CO_2} compared to k_{CO_2} at the *in situ* temperature (Figure 5 vs. Figure S5 in Supplemental
160 information). In Section 3.4, the relationship between CO_2 and DMS gas transfer velocities
161 and wind speed is examined using $k_{DMS,Sc}$ and k_{CO_2} .

162 **2.3 Calculation of k_{bub,CO_2}**

163 The flux of a water-side controlled gas is equal to the sum of the interfacial flux and the bubble-
164 mediated flux. For gases with significant air/sea disequilibrium these processes are often
165 considered as parallel transfer velocities, i.e. total transfer velocity $k_w = k_{int} + k_{bub}$. See Woolf
166 (1997) for a more complete discussion of bubble-mediated transfer for gases close to
167 ocean/atmosphere equilibrium. We assume that turbulence and diffusive mixing at the sea
168 surface operate similarly upon the interfacial air/sea transfer of CO_2 and DMS (i.e. $k_{int,CO_2} =$
169 $k_{int,DMS}$), given appropriate normalization for the differences in molecular diffusivity. Observed
170 differences between $k_{DMS,Sc}$ and k_{CO_2} should therefore be a measure of the difference between
171 the bubble-mediated contributions to DMS and CO_2 gas transfer:

$$172 \quad \Delta k_w = k_{bub,CO_2} - k_{bub,DMS} \quad \text{Equation 5}$$

173 Strictly speaking, Equation 5 should also account for the influence of bubble overpressure,
174 which alters the gas flux due to bubbles when the concentration gradient is into the ocean. The
175 extra pressure on the gas in the bubbles is calculated following Woolf (1997): $\Delta = (U_{10}/U_i)^2 \%$
176 where U_i is the wind speed at which the supersaturation of a particular gas equals 1% (49 m s⁻¹
177 in the case of CO₂). A high wind speed (20 m s⁻¹) gives $\Delta = 0.167\%$, which would lead to
178 only a ~2% enhancement of the CO₂ flux when the air/sea concentration gradient is 30 ppm
179 (minimum for this study) and into the ocean. The magnitude of this effect would be larger for
180 gases less soluble than CO₂ but we are able to ignore it for the purposes of this study.

181 k_{bub,CO_2} and $k_{bub,DMS}$ are related by the influence of solubility and diffusivity upon bubble-
182 mediated transfer. We parameterize this relationship simply as $k_{bub,DMS} = f \cdot k_{bub,CO_2}$.
183 Substitution into Equation 5 yields:

$$184 \quad k_{bub,CO_2} = \frac{\Delta k_w}{1 - f} \quad \text{Equation 6}$$

185 The value of f depends on seawater temperature and the complex dynamics of bubble formation
186 and cycling (size distributions, surfactants, etc.). At the mean SST encountered in this study
187 (9.8°C), the bubble gas transfer models of Woolf (Woolf, 1997) and Asher (Asher and
188 Wanninkhof, 1998; Asher et al., 2002) yield values for f of 0.14 and 0.28, respectively (see
189 Supplemental information for model equations).

190 **2.4 Sea surface imaging**

191 Whitecap areal fraction was measured using images of the sea surface recorded with a digital
192 camera (5 mega pixel Arecont Vision, 16 mm focal length lens) mounted 14.6 m above the
193 ocean surface at an angle of ~75° from the nadir. Image footprints represent ~7600 m² of sea
194 surface. Images were collected at a sample period of about 1 second and post-processed for
195 whitecap fraction according to the Automated Whitecap Extraction algorithm method
196 (Callaghan and White, 2009). More detail on the methodology, camera exposure settings and
197 data comparability are provided in the Supplemental information. Images were further
198 processed to distinguish whitecap pixels as either stage A or stage B whitecaps by applying a
199 spatial separation technique (Scanlon and Ward, 2013). The whitecap fraction measurements
200 were averaged in the same way as the gas transfer velocities (i.e. time-averaged mean values
201 as well as 2 m s⁻¹ wind speed bins).

202 **3 Results**

203 **3.1 Cruise location and environmental conditions**

204 This study took place in the summertime North Atlantic (June 24 – July 18, 2011; DOY 175-
205 199), departing and returning to Woods Hole, MA. Most of the data were collected north of
206 50°N, including the occupation of four 24-36 hr stations – ST181, ST184, ST187 and ST191
207 (Figure 1). The cruise track was designed to sample regions with high biological productivity
208 and phytoplankton blooms, with large air/sea concentration differences for CO₂ and DMS. The
209 cruise meteorology and physical oceanography is discussed in detail by (Bell et al., 2013). A
210 series of weather systems travelling from West to East passed over the region during the cruise.
211 Wind speeds ranged from ~1 to 22 m s⁻¹, with strongest winds during the frontal passages at
212 stations ST184 and ST191 (Figure 1b). Atmospheric boundary layer stability was close to
213 neutral for most of the cruise ($|z/L| < 0.07$; 75% of the time), with infrequent stable conditions
214 ($z/L > 0.05$; <8% of the time, Figure 1a). There was no evidence that the stable periods affected
215 the flux measurements (Bell et al., 2013). Whitecap areal fraction increased up to a maximum
216 of ~0.06 in response to high wind speeds (Figure 1b).

217 **3.2 Whitecaps**

218 Whitecaps were observed during Knorr_11 when wind speeds exceeded 4.5 m s⁻¹, a typical
219 wind speed threshold for whitecap formation in the open ocean (Callaghan et al., 2008;
220 Schwendeman and Thomson, 2015). Whitecap areal fraction is a strong, non-linear function
221 of wind speed (Figure 2a). The whitecap vs. wind speed relationship for Knorr_11 is similar in
222 shape to recently-published, wind speed-based whitecap parameterisations (Callaghan et al.,
223 2008; Schwendeman and Thomson, 2015). At intermediate wind speeds the Knorr_11
224 whitecap data are lower than the parameterisations (Figure 2a). Total whitecap coverage is a
225 function of (i) active ‘stage A whitecaps’ (W_A) produced from recent wave breaking and (ii)
226 maturing ‘stage B whitecaps’ (W_B) that are decaying foam from previous breakers. The Stage
227 A whitecap fraction data is highly variable at ~11 m s⁻¹ wind speeds (Figure 2b), which is
228 driven by the difference in the wind-wave conditions during Knorr_11 (see discussion in
229 Supplemental information).

230 3.3 Concentrations, fluxes and gas transfer velocities

231 Seawater pCO₂ was consistently lower than the overlying atmosphere throughout the study
232 region due to biological uptake (Figure 3a). As a result, the air/sea concentration difference
233 ($\Delta p\text{CO}_2$) was large and always into the ocean, with $\Delta p\text{CO}_2 < -45$ ppm for more than 80% of the
234 measurements. Periods with particularly enhanced $\Delta p\text{CO}_2$ into the ocean were during the
235 transit between ST181 and ST184 ($\Delta p\text{CO}_2$ as large as -120 ppm) and during ST191 ($\Delta p\text{CO}_2$
236 consistently -75 ppm).

237 Seawater DMS levels were much higher than atmospheric levels, reflecting the biogenic
238 sources in seawater and the relatively short atmospheric lifetime (~1 day; Kloster et al., 2006).
239 The largest air/sea DMS concentration differences (ΔDMS) of 6-12 ppb were observed during
240 DOY 185-190 (Figure 4a). The ΔDMS and $\Delta p\text{CO}_2$ did not co-vary (Spearman $\rho = 0.11$, $n=918$,
241 $p < 0.001$). This is not surprising because, although seawater DMS and CO₂ signals are both
242 influenced by biological activity, they are controlled by different processes. Seawater CO₂
243 levels reflect the net result of community photosynthesis and respiration, while DMS
244 production is related to metabolic processes that are highly species-dependent (Stefels et al.,
245 2007).

246 CO₂ fluxes (F_{CO_2}) were generally into the ocean, as expected given the direction of the air/sea
247 concentration difference (Figure 3b). The variability in F_{CO_2} observed on this cruise reflects
248 dependence on both wind speed and $\Delta p\text{CO}_2$. For example, during DOY182 air-to-sea CO₂
249 fluxes increase due to a gradual increase in $\Delta p\text{CO}_2$ with fairly constant wind speed. More
250 commonly, $\Delta p\text{CO}_2$ was fairly constant and variability in F_{CO_2} reflected changes in wind speed.
251 For example, from DOY 185-187 wind speeds gradually declined from ~10 to 5 m s⁻¹ with a
252 concurrent decline in F_{CO_2} . DMS eddy covariance fluxes were always out of the ocean. Ten
253 minute averaged DMS fluxes (F_{DMS}) clearly show the influence of ΔDMS (e.g. DOY 188) and
254 wind speed (e.g. DOY 184).

255 Gas transfer velocities of CO₂ and DMS from this cruise exhibit two systematic differences: i)
256 k_{DMS} values are generally lower than k_{CO_2} , particularly during episodes of high wind speed;
257 and ii) k_{CO_2} is characterized by much larger scatter than k_{DMS} . We attribute the large scatter in
258 k_{CO_2} to the greater random uncertainty associated with the eddy covariance measurement of
259 air/sea CO₂ fluxes compared to those of DMS. As shown by Miller et al. (2010), the analytical

260 approach used in this study (dried air, closed path LI7500) has sufficient precision to
261 adequately resolve the turbulent fluctuations in atmospheric CO₂ associated with the surface
262 flux over most of the cruise ($\Delta p\text{CO}_2 < -30$ ppm). The scatter in the CO₂ flux measurements is
263 more likely due to environmental variability resulting from fluctuations in boundary layer CO₂
264 mixing ratio arising from horizontal and/or vertical transport unrelated to air/sea flux (Edson
265 et al., 2008; Blomquist et al., 2014). These effects likely have a much smaller effect on air/sea
266 DMS fluxes, because the air/sea DMS concentration difference is always much larger than the
267 mean atmospheric DMS concentration (due to the short atmospheric lifetime of DMS). For
268 example, a $\Delta p\text{CO}_2$ of 100 ppm at a wind speed of 10 m s⁻¹ will produce turbulent fluctuations
269 that are ~0.02% of the background CO₂ on average. In contrast, a typical seawater DMS
270 concentration (2.6 nM) at a wind speed of 6 m s⁻¹ generates fluctuations that are 20% of the
271 background (Table 1; Blomquist et al., 2012). Thus, F_{CO_2} measurements are highly sensitive
272 to small fluctuations in background CO₂ and the relative uncertainty is expected to be much
273 larger than that for F_{DMS} .

274 **3.4 Comparison of k_{CO_2} and $k_{\text{DMS},sc}$**

275 The differences between CO₂ and DMS gas transfer velocities observed in the time series are
276 also evident when the data are examined as a function of wind speed. From the 10-minute
277 averaged data, it is clear that k_{CO_2} is greater than k_{DMS} and has a stronger wind speed-
278 dependence over most of the wind speed range (Figure 5a,b). These broad trends are also easily
279 seen in longer time-averaged data. Flux and ΔC measurements were averaged into 2 hour
280 periods (minimum of 3 flux intervals per 2 hour period), which reduced the scatter in F_{CO_2}
281 while preserving the temporal variability (see Figure S7 in Supplemental information). Gas
282 transfer velocities were then recalculated from the 2 hour averaged data. 10-minute k_{CO_2} and
283 $k_{\text{DMS},sc}$ data were also averaged into 2 m s⁻¹ wind speed bins, with a minimum of five 10-minute
284 periods per bin. The 2 hour averaged data and the wind speed binned data show k_{CO_2} and $k_{\text{DMS},sc}$
285 diverging at intermediate wind speeds, differing by a factor of roughly two at 10 m s⁻¹ (Figure
286 5c,d).

287 DMS gas transfer velocities on this cruise exhibit complex behaviour at intermediate to high
288 wind speeds, as discussed in Bell et al. (2013). $k_{\text{DMS},sc}$ increases linearly with wind speed up
289 to ~11 m s⁻¹ (Figure 5). Under the sustained high wind, high wave conditions encountered

290 during ST191, the wind speed-dependence of $k_{DMS,Sc}$ was lower than expected, with a slope
291 roughly half that of the rest of the cruise data. This effect was not observed at ST184 – for
292 detailed discussion, see Bell et al. (2013). Such coherent spatial-temporal variation means that
293 wind speed bin averaging of the higher wind speed $k_{DMS,Sc}$ may mask real variability in the
294 relationship with wind speed. Relationships developed from wind speed bin-averaged gas
295 transfer data should be interpreted with caution, especially when it comes to developing
296 generalizable air/sea gas transfer models.

297 The Knorr_11 k_{CO_2} data also demonstrate a clear wind speed dependence (Figure 5). The
298 NOAA COARE model for CO₂ has been tuned to previous eddy covariance flux measurements
299 (McGillis et al., 2001), with bubble-mediated transfer determining the non-linear relationship
300 with wind speed (Fairall et al., 2011). There is reasonable agreement between the COARE
301 model gas transfer velocity predictions and the Knorr_11 k_{CO_2} data up to ~ 11 m s⁻¹ wind speed.
302 Above 11 m s⁻¹, the COARE model over predicts k_{CO_2} . This could be interpreted as indicating
303 high wind speed suppression of gas transfer for CO₂ as observed for DMS (as discussed by
304 Bell et al., 2013). However, it is important to note that the number of high wind speed (>15 m
305 s⁻¹) gas transfer measurements in this study is limited to 9 hours and 16 hours of data for DMS
306 and CO₂ respectively. Much more data are needed in order to firmly establish the high wind
307 speed behaviour.

308 The COAREG 3.1 model parameterizes interfacial gas transfer by scaling to Sc and friction
309 velocity and estimates bubble-mediated gas transfer following Woolf (1997). The lower
310 solubility of CO₂ leads to enhanced gas transfer relative to that of DMS at high wind speeds
311 where bubble transport is significant (Fairall et al., 2011). There is good agreement between
312 the COAREG model gas transfer velocity predictions and the Knorr_11 k_{CO_2} and k_{DMS} data
313 until ~ 11 m s⁻¹ wind speed.

314 Earlier in this paper we introduced the quantity Δk_w as an observational measure of the
315 difference in gas transfer velocities of CO₂ and DMS (Section 2.3, Equation 6). The
316 relationship between Δk_w and wind speed is positive and shows no systematic differences
317 related to temporal variability (Figure 6). Sea surface temperature (SST) is indicated by symbol
318 size. Some of the scatter in Figure 6 could be driven by changes in Sc due to SST variability.
319 Nearly all of the data in Figure 6 are from periods when SST was relatively constant

320 (9.7±1.1°C). Many of the k_{CO_2} data with warm seawater (i.e. ST181, SST > 12°C) were
321 rejected by our quality control criteria (see Appendix A.3). These data were collected when
322 wind speeds were low, which resulted in small CO₂ fluxes with large variability at low
323 frequencies. Of the periods with SST > 12°C that passed the quality control criteria, the
324 majority contributed fewer data within a 2 hour averaging period than the minimum threshold
325 (three 10-minute averaged data points).

326 4 Discussion

327 The bubble-mediated component of gas transfer is a strong function of wind speed and breaking
328 waves. Previous estimates of bubble-mediated air/sea gas exchange have used data from
329 laboratory experiments (Keeling, 1993; Asher et al., 1996; Woolf, 1997). The differences
330 between gas transfer velocities for DMS and CO₂ provide a unique way to constrain the
331 importance of bubble-mediated transfer under natural conditions. This study shows that Δk_w is
332 near zero (< 4.5 cm hr⁻¹) at low wind speeds ($U_{10} \leq 4.5$ m s⁻¹), which is consistent with the wind
333 speed at which whitecap fraction becomes significant ($W_T > 10^{-5}$, Figure 2a). Above 4.5 m s⁻¹,
334 Δk_w increases non-linearly, consistent with an increase in bubble-mediated CO₂ transfer
335 associated with wave breaking. The relationship between Δk_w and wind speed is non-linear, and
336 a power law wind speed-dependence yields a good fit ($R^2 = 0.66$; Figure 6):

$$337 \quad \Delta k_w = 0.177U_{10}^{1.928} \quad \text{Equation 7}$$

338 The functional form of this relationship is qualitatively consistent with those found between
339 U_{10} and breaking waves/wave energy dissipation (Melville and Matusov, 2002) and U_{10} vs.
340 whitecap areal fraction (e.g. Callaghan et al., 2008; Schwendeman and Thomson, 2015).
341 Bubble-mediated gas transfer is the only viable explanation for the magnitude and wind-speed
342 dependence of Δk_w . The only alternative explanation would require a large systematic bias in
343 the measurement of relative gas transfer velocities of DMS and CO₂. There are no obvious
344 candidates for such biases.

345 During strong wind/large wave conditions, the Knorr_11 data suggest that bubble-mediated
346 exchange is a dominant contributor to the total transfer of CO₂. For example, when wind speeds
347 were 11-12 m s⁻¹, Δk_w was about 50% of the total CO₂ gas transfer (k_{CO_2}). A significant
348 contribution by bubbles to the total gas transfer velocity means that bubble-mediated exchange
349 must be included and adequately parameterised by gas transfer models. The Schmidt number

350 (Sc) normalisation (Equation 4) assumes that the gas transfer velocity is purely interfacial. An
351 alternative normalisation (involving Sc and solubility) is required when bubble-mediated
352 transfer is significant. Our data suggest that the current Sc normalisation should be applied with
353 caution to gas transfer data for different solubility gases at wind speeds greater than 10 m s^{-1} .

354 If Δk_w reflects the difference between the bubble-mediated contribution to the transfer of CO_2
355 and DMS, one would expect Δk_w to correlate with wave-breaking, and hence with the areal
356 coverage of whitecaps. Breaking waves generate plumes of bubbles (Stage A whitecaps, W_A),
357 which then rise to the surface and persist for a short period as foam (Stage B whitecaps, W_B).
358 Almost all whitecap measurements represent the fraction of the sea surface that is covered by
359 bubble plumes and/or foam i.e. $W_T = W_A + W_B$. Δk_w is positively correlated with both W_T
360 (Spearman $\rho = 0.65$, $n=43$, $p<0.001$) and W_A (Spearman $\rho = 0.74$, $n=32$, $p<0.001$) (Figure 7a,b).
361 These correlations are approximately the same strength as the correlation between Δk_w and
362 wind speed (Spearman $\rho = 0.73$, $n=88$, $p<0.001$). The functional form of the relationship
363 between Δk_w and whitecap areal extent appears to be linear for $W_T > 0.005$. However, the
364 Knorr_11 dataset is small and quite scattered, particularly when $W_T < 0.005$. More data are
365 required to fully test the validity of whitecap areal fraction as a proxy for bubbles and bubble-
366 mediated exchange.

367 Observations of the decaying white cap signal (W_B) suggest that the persistence of surface foam
368 is related to both bubble plume depth (deeper bubble plumes take longer to degas) and sea
369 surface chemistry (Callaghan et al., 2013). As measured here, W_B is approximately an order of
370 magnitude larger than W_A and thus dominates the W_T signal. It is often assumed that gas
371 exchange takes place in bubble plumes formed by active wave breaking (i.e. W_A), while W_B
372 may vary widely due to surfactant concentration with little or no impact upon bubble-mediated
373 gas exchange (e.g. Pereira et al., 2016). In this case, Δk_w should be more strongly correlated
374 with W_A than W_B or W_T . The Knorr_11 data do not suggest that W_A is an improvement upon
375 either W_T or even wind speed as a measure of bubble mediated exchange. This may be because
376 whitecaps do not fully represent the bubbles facilitating gas exchange as these may dissolve
377 before they reach the sea surface. Alternatively, W_T and W_A may be equally good (or poor)
378 proxies for bubbles because: (i) surfactant activity was either insignificant or sufficiently
379 invariant in the study region (despite high biological productivity) that W_B does not confound
380 the relationship between W_T and W_A ; (ii) W_A is no better than W_T at representing the volume of

381 air entrained by breaking waves; and/or (iii) bubbles residing at the surface (i.e. W_B) continue
382 to contribute to gas transfer (Goddijn-Murphy et al., 2016).

383 As shown earlier, the bubble-mediated contribution to gas transfer (k_{bub,CO_2}) can be obtained
384 from Δk_w using information from mechanistic bubble gas transfer models (f , see Section 2.3).
385 The k_{bub,CO_2} datasets derived from the Knorr_11 data using the Asher (Asher and Wanninkhof,
386 1998; Asher et al., 2002) and Woolf (Woolf, 1997) models differ by about 15% (Figure 8). The
387 field-based estimates of k_{bub,CO_2} can also be compared to model-only estimates for the Knorr_11
388 conditions using the Asher and Woolf models. Both models are based on total whitecap areal
389 fraction, W_T . A non-linear fit of the Knorr_11 W_T and wind speed measurements ($W_T = 1.9 \times 10^{-6}$
390 $U_{10m}^{3.36}$) was used to drive both models (Figure 8). Asher et al. (2002) is based on laboratory
391 tipping bucket gas evasion experiments (Asher et al., 1996) and the model was then adjusted
392 to represent the flux of CO_2 into the ocean (invasion). Woolf (1997) scaled a single bubble
393 model to the open ocean based on laboratory experiments.

394 Both models significantly underestimate k_{bub,CO_2} at wind speeds below about 11 m s^{-1} . At higher
395 wind speeds, the Asher et al. (2002) model increases rapidly with wind speed to agree better
396 with the Knorr_11 data. In contrast, Woolf (1997) consistently underestimates k_{bub,CO_2} at all
397 wind speeds. Both k_{bub,CO_2} models depend on the choice of wind speed-whitecap
398 parameterisation. Using the Schwendeman and Thomson (2015) whitecap parameterisation
399 instead of the Knorr_11 best fit makes some difference to the model output, but not enough to
400 adequately fit to the data (Figure 8). A ‘dense plume model’ was also developed by Woolf et
401 al. (2007) to take account of the interaction of a bubble plume with the interstitial water
402 between bubbles. This model yields estimates of k_{bub,CO_2} that are even lower than the original
403 Woolf (1997) ‘single bubble model’ (data not shown).

404 It is likely that the Knorr_11 cruise data will be compared with estimates of k_{bub,CO_2} derived
405 from future field campaigns, which will be conducted under different environmental
406 conditions. Our k_{bub,CO_2} data is at *in situ* seawater temperature ($\sim 10^\circ\text{C}$) and thus *in situ* CO_2
407 solubility ($\alpha=1.03$) and diffusivity ($Sc=1150$). We use the Asher et al. (2002) and Woolf (1997)
408 bubble models to make estimates of k_{bub,CO_2} normalised to a standard seawater temperature of

409 20°C ($k_{bub,CO_2,20^\circ C}$, where $\alpha=0.78$ and $Sc=666$). The 2 hour averaged Knorr_11 cruise data,
410 including estimates of Δk_w , k_{bub,CO_2} and $k_{bub,CO_2,20^\circ C}$, are provided in Supplemental Table S1.
411 The approach used in this study to estimate Δk_w and k_{bub,CO_2} from the Knorr_11 field data
412 neglects the effect of sea surface skin temperature and CO₂ chemical enhancement. Skin
413 temperature is typically only a few tenths of a degree less than bulk seawater under the
414 conditions encountered in this study (Fairall et al., 1996). The impact upon k_{CO_2} due to skin
415 temperature effects on CO₂ solubility and carbonate speciation is likely on the order of 3%
416 (Woolf et al., 2016). There is a chemical enhancement of the CO₂ flux due to ionization at the
417 sea surface (Hoover and Berkshire, 1969). The effect on k_{CO_2} has been estimated to be up to
418 about 8% at a wind speed of 4-6 m s⁻¹ (Wanninkhof and Knox, 1996), which amounts to a
419 maximum impact of a few cm hr⁻¹. By neglecting these effects we have slightly overestimated
420 Δk_w and k_{bub,CO_2} , but the magnitude of these corrections would be small relative to the
421 environmental scatter or measurement uncertainty.

422 5 Conclusions

423 The Knorr_11 concurrent measurements of DMS and CO₂ gas transfer velocities show
424 significant differences in gas transfer between the two gases at intermediate-high wind speeds.
425 These data indicate that: i) bubble-mediated gas transfer becomes significant for CO₂ at or
426 above the threshold for wave-breaking; and ii) the wind speed-dependence is non-linear, with
427 a similar functional form to proposed relationships predicting whitecap areal extent from wind
428 speed. However, existing models of bubble-mediated gas transfer using the Knorr_11 *in situ*
429 observations of whitecap fraction significantly underestimate the importance of this process.

430 There are a number of assumptions behind model estimates of bubble-mediated gas exchange
431 (Goddijn-Murphy et al., 2016). Model bias can be crudely split into: i) uncertainties in the
432 scaling of whitecap fraction to the bubble population (e.g. using Cipriano and Blanchard,
433 1981); and ii) the relationship between gas exchange and bubble properties, which are predicted
434 as a function of air entrainment into the surface ocean by a breaking wave, bubble injection
435 depth, size distribution and mobility through the water (a function of surface cleanliness and
436 surfactants). The underestimation of bubble-mediated CO₂ gas transfer by both models is
437 particularly apparent at low-intermediate wind speeds and low whitecap fraction. This could

438 indicate that either bubble production during microscale breaking is an important process for
439 gas transfer or the relationship between whitecap fraction and the bubble population is poorly
440 constrained.

441 In summary, the approach of using simultaneous measurements of multiple gases with different
442 solubility appears to be a viable way to constrain the magnitude of bubble-mediated gas
443 transfer. Analysis of additional sparingly soluble gases, such as methane or oxygenated
444 hydrocarbons would further strengthen this approach. A much larger data set, under a wider
445 range of oceanographic conditions is certainly needed. In particular, it would be useful to
446 examine DMS and CO₂ gas transfer velocities in ocean regions with different temperatures,
447 where the solubility of each gas is significantly different from this study.

448

449 **Appendix A**

450 **A.1 Seawater CO₂ and DMS measurements**

451 Seawater CO₂ and DMS were monitored in the supply of seawater pumped continuously
452 through the ship from an intake on the bow located 6 m below the sea surface. CO₂ was
453 equilibrated with air in a recirculating showerhead-type system. Alternate air and water side
454 pCO₂ were each measured for 5 min by the same Infrared Gas Analyser (IRGA). Seawater
455 DMS was equilibrated with DMS-free air in a tubular porous membrane equilibrator, operated
456 in a single-pass, counterflow mode. DMS was measured at 1 Hz using chemical ionization
457 mass spectrometry and bin-averaged at 1 minute intervals (UCI miniCIMS; Saltzman et al.,
458 2009). DMS was calibrated by continuously pumping an internal standard of tri-deuterated,
459 DMS (d₃-DMS) into the seawater flow just before the equilibrator. Details of the methods and
460 instrumentation used for equilibration and detection of seawater DMS are described in
461 Saltzman et al. (2009).

462 **A.2 Mast-mounted instrumentation and data acquisition**

463 The eddy covariance system was mounted 13.6 m above the sea surface on the bow mast.
464 Platform angular rates and accelerations were measured by two Systron Donner Motion Pak II
465 (MPII) units. Three dimensional winds and sonic temperature were measured by two Campbell
466 CSAT3 sonic anemometers. Air sampling inlets for DMS and CO₂ were located at the same

467 height as the anemometers and within 20 cm of the measurement region. GPS and digital
468 compass output were digitally logged at 1 Hz. Winds were corrected for ship motion and
469 orientation as described in Miller et al. (2008) and Landwehr et al. (2015). The eddy covariance
470 data streams were logged in both analog and digital format as described in Bell et al. (2013).

471 **A.3 High frequency atmospheric DMS and CO₂ measurements**

472 Atmospheric DMS measurements were made at 10 Hz using an atmospheric pressure chemical
473 ionisation mass spectrometer located in a lab van (UCI mesoCIMS; Bell et al. (2013)). Air
474 was drawn to the instrument through a 28 m long ½ in OD Teflon tube. A subsample of the
475 air stream was passed through a Nafion drier prior to entering the mass spectrometer. The
476 measurement was calibrated using an internal gas standard of tri-deuterated DMS added to the
477 inlet (see Bell et al., 2013).

478 Atmospheric CO₂ measurements were made on air drawn at 8 L min⁻¹ through a filtered inlet
479 (90 mm diameter with 1 micron pore size, Savillex) near the sonic anemometers on the bow
480 mast, through 5 m of 5.9 mm ID polyethylene-lined Dekabon tubing to two fast-response
481 CO₂/H₂O IRGAs in an enclosure on the bow mast. The IRGAs were open-path style sensors
482 (LI7500, Licor Inc.) converted to a closed-path configuration (see Miller et al., 2010) and were
483 plumbed in series. A Nafion multi-tube membrane drier (PD-200T, PermaPure) with 6 L min⁻¹
484 dry air counter flow was installed between the two IRGAs such that the upstream IRGA
485 sampled undried air and the downstream IRGA sampled the same air after drying. This
486 technique removes 97% of the Webb Correction from the measured CO₂ flux (first shown by
487 Miller et al. (2010) and confirmed by Landwehr et al. (2014)).

488 The air flow through both the CO₂ and DMS inlets was fully turbulent (Re > 10,000). The inlets
489 used in this study introduced a small delay ($\Delta t = 2.2$ s for DMS, $\Delta t = 1.2$ s for CO₂) between
490 measured wind and atmospheric measurements, as well as minor loss of covariance at high
491 frequencies (<5%). The methods used to estimate the delay and loss of flux are given in Bell
492 et al. (2013).

493 Eddy covariance fluxes were computed for DMS and CO₂ as F_{DMS} or $F_{CO_2} = \sigma_{air} \langle w'c' \rangle$

494 where σ_{air} is the dry air density, w' is the fluctuation in vertical winds and c' is the delay-
495 adjusted fluctuation in gas concentration. Average covariance fluxes were processed in 10
496 minute and 9.5 minute intervals for DMS and CO₂, respectively (hereafter referred to as 10

497 minute intervals). Momentum and sensible heat fluxes were also computed for 10 minute
498 intervals (see Bell et al., 2013).

499 Sampling intervals with a mean wind direction relative to the bow of $>90^\circ$ were excluded from
500 the final data set. CO_2 fluxes were also excluded from intervals when either: i) relative wind
501 direction changed excessively ($\text{SD} > 10^\circ$); ii) relative wind speed was low ($< 1 \text{ m s}^{-1}$); or iii)
502 ΔCO_2 was low ($< |30| \text{ ppm}$). DMS and CO_2 fluxes were quality controlled for excessive low
503 frequency flux as described in the Supplemental information of Bell et al. (2013). These quality
504 control criteria excluded 62% of the intervals for CO_2 and 55% for DMS and significantly
505 reduced the scatter in the data.

506

507 *Acknowledgements.* We thank the Captain and crew of the R/V Knorr and the Woods Hole
508 Marine Department for their assistance in carrying out this cruise. Funding for this research
509 was provided by the NSF Atmospheric Chemistry Program (AGS-0851068, -0851472, -
510 0851407 and -1134709) and the NSF Independent Research and Development program. A. C.
511 acknowledges support from a Royal Society Shooter International Fellowship and from the
512 National Science Foundation under grant OCE-1434866. B. W. acknowledges support from
513 Science Foundation Ireland under grant 08/US/I1455 and from the FP7 Marie Curie
514 Reintegration programme under grant 224776. We are grateful for constructive comments from
515 our reviewers (Byron Blomquist, Ian Brooks and Bill Asher), which helped improve the paper.
516 This study is a contribution to the international Surface Ocean Lower Atmosphere Study
517 (SOLAS) programme.

518

519 **References**

- 520 Asher, W. E., Karle, L. M., Higgins, B. J., Farley, P. J., Monahan, E. C., and Leifer, I. S.: The influence of bubble
521 plumes on air-seawater gas transfer velocities, *J Geophys Res-Oceans*, 101, 12027-12041, 1996.
- 522 Asher, W. E., and Wanninkhof, R.: The effect of bubble-mediated gas transfer on purposeful dual-gaseous tracer
523 experiments, *Journal of Geophysical Research: Oceans*, 103, 10555-10560, 10.1029/98jc00245, 1998.
- 524 Asher, W. E., Edson, J., McGillis, W., Wanninkhof, R., Ho, D. T., and Litchendor, T.: Fractional area whitecap
525 coverage and air-sea gas transfer velocities measured during GasEx-98, in: *Gas Transfer at Water Surfaces*,
526 American Geophysical Union, 199-203, 2002.
- 527 Bell, T. G., de Bruyn, W., Miller, S. D., Ward, B., Christensen, K., and Saltzman, E. S.: Air/sea DMS gas transfer
528 in the North Atlantic: evidence for limited interfacial gas exchange at high wind speed, *Atm Chem Phys*, 13,
529 11073-11087, 2013.

530 Bell, T. G., de Bruyn, W., Marandino, C. A., Miller, S. D., Law, C. S., Smith, M. J., and Saltzman, E. S.:
531 Dimethylsulfide gas transfer coefficients from algal blooms in the Southern Ocean, *Atm Chem Phys*, 15, 1783-
532 1794, 10.5194/acp-15-1783-2015, 2015.

533 Blomquist, B. W., Fairall, C. W., Huebert, B. J., Kieber, D. J., and Westby, G. R.: DMS sea-air transfer velocity:
534 Direct measurements by eddy covariance and parameterization based on the NOAA/COARE gas transfer model,
535 *Geophysical Research Letters*, 33, art. no.-L07601, 10.1029/2006gl025735, 2006.

536 Blomquist, B. W., Fairall, C. W., Huebert, B. J., and Wilson, S. T.: Direct measurement of the oceanic carbon
537 monoxide flux by eddy correlation, *Atmos Meas Tech*, 5, 3069-3075, 10.5194/amt-5-3069-2012, 2012.

538 Blomquist, B. W., Huebert, B. J., Fairall, C. W., Bariteau, L., Edson, J. B., Hare, J. E., and McGillis, W. R.:
539 Advances in air-sea CO₂ flux measurement by eddy correlation, *Boundary-Layer Meteorology*, 152, 245-276,
540 10.1007/s10546-014-9926-2, 2014.

541 Callaghan, A. H., de Leeuw, G., Cohen, L., and O'Dowd, C. D.: Relationship of oceanic whitecap coverage to
542 wind speed and wind history, *Geophysical Research Letters*, 35, L23609, 10.1029/2008gl036165, 2008.

543 Callaghan, A. H., and White, M.: Automated processing of sea surface images for the determination of whitecap
544 coverage, *Journal of Atmospheric and Oceanic Technology*, 26, 383-394, 10.1175/2008jtecho634.1, 2009.

545 Callaghan, A. H., Deane, G. B., and Stokes, M. D.: Two regimes of laboratory whitecap foam decay: Bubble-
546 plume controlled and surfactant stabilized, *Journal of Physical Oceanography*, 43, 1114-1126, 10.1175/Jpo-D-12-
547 0148.1, 2013.

548 Carpenter, L. J., Archer, S. D., and Beale, R.: Ocean-atmosphere trace gas exchange, *Chem Soc Rev*, 41, 6473-
549 6506, 10.1039/c2cs35121h, 2012.

550 Cipriano, R. J., and Blanchard, D. C.: Bubble and aerosol spectra produced by a laboratory 'breaking wave',
551 *Journal of Geophysical Research: Oceans*, 86, 8085-8092, 10.1029/JC086iC09p08085, 1981.

552 Dacey, J. W. H., Wakeham, S. G., and Howes, B. L.: Henry's law constants for dimethylsulfide in fresh water and
553 seawater, *Geophysical Research Letters*, 11, 991-994, 1984.

554 Edson, J. B., DeGrandpre, M. D., Frew, N. M., and McGillis, W. R.: Investigations of air-sea gas exchange in the
555 CoOP Coastal Air-Sea Chemical Exchange Project, *Oceanography*, 21, 34-45,
556 <http://dx.doi.org/10.5670/oceanog.2008.03>, 2008.

557 Fairall, C. W., Bradley, E. F., Godfrey, J. S., Wick, G. A., Edson, J. B., and Young, G. S.: Cool-skin and warm-
558 layer effects on sea surface temperature, *J Geophys Res-Oceans*, 101, 1295-1308, 10.1029/95jc03190, 1996.

559 Fairall, C. W., Yang, M., Bariteau, L., Edson, J. B., Helmig, D., McGillis, W., Pezoa, S., Hare, J. E., Huebert, B.,
560 and Blomquist, B.: Implementation of the Coupled Ocean-Atmosphere Response Experiment flux algorithm with
561 CO₂, dimethyl sulfide, and O₃, *J Geophys Res-Oceans*, 116, C00F09, 10.1029/2010jc006884, 2011.

562 Goddijn-Murphy, L., Woolf, D. K., and Marandino, C.: Space-based retrievals of air-sea gas transfer velocities
563 using altimeters: Calibration for dimethyl sulfide, *J Geophys Res-Oceans*, 117, 10.1029/2011jc007535, 2012.

564 Goddijn-Murphy, L., Woolf, D. K., Callaghan, A. H., Nightingale, P. D., and Shutler, J. D.: A reconciliation of
565 empirical and mechanistic models of the air-sea gas transfer velocity, *Journal of Geophysical Research: Oceans*,
566 121, 818-835, 10.1002/2015jc011096, 2016.

567 Hoover, T. E., and Berkshire, D. C.: Effects of hydration on carbon dioxide exchange across an air-water interface,
568 *Journal of Geophysical Research*, 74, 456-464, 1969.

569 Huebert, B. J., Blomquist, B. W., Hare, J. E., Fairall, C. W., Johnson, J. E., and Bates, T. S.: Measurement of the
570 sea-air DMS flux and transfer velocity using eddy correlation, *Geophysical Research Letters*, 31, L23113,
571 10.1029/2004gl021567, 2004.

572 Keeling, R. F.: On the role of large bubbles in air-sea gas exchange and supersaturation in the ocean, *Journal of*
573 *Marine Research*, 51, 237-271, 10.1357/0022240933223800, 1993.

574 Kloster, S., Feichter, J., Reimer, E. M., Six, K. D., Stier, P., and Wetzol, P.: DMS cycle in the marine ocean-
575 atmosphere system - a global model study, *Biogeosciences*, 3, 29-51, 2006.

576 Landwehr, S., Miller, S. D., Smith, M. J., Saltzman, E. S., and Ward, B.: Analysis of the PKT correction for direct
577 CO₂ flux measurements over the ocean, *Atm Chem Phys*, 14, 3361-3372, 10.5194/acp-14-3361-2014, 2014.

578 Landwehr, S., O'Sullivan, N., and Ward, B.: Direct flux measurements from mobile platforms at sea: Motion and
579 airflow distortion corrections revisited, *Journal of Atmospheric and Oceanic Technology*, 32, 1163-1178,
580 10.1175/jtech-d-14-00137.1, 2015.

581 Le Quéré, C., Moriarty, R., Andrew, R. M., Peters, G. P., Ciais, P., Friedlingstein, P., Jones, S. D., Sitch, S., Tans,
582 P., Arneeth, A., Boden, T. A., Bopp, L., Bozec, Y., Canadell, J. G., Chini, L. P., Chevallier, F., Cosca, C. E., Harris,
583 I., Hoppema, M., Houghton, R. A., House, J. I., Jain, A. K., Johannessen, T., Kato, E., Keeling, R. F., Kitidis, V.,
584 Klein Goldewijk, K., Koven, C., Landa, C. S., Landschützer, P., Lenton, A., Lima, I. D., Marland, G., Mathis, J.
585 T., Metzl, N., Nojiri, Y., Olsen, A., Ono, T., Peng, S., Peters, W., Pfeil, B., Poulter, B., Raupach, M. R., Regnier,
586 P., Rödenbeck, C., Saito, S., Salisbury, J. E., Schuster, U., Schwinger, J., Séférian, R., Segschneider, J., Steinhoff,
587 T., Stocker, B. D., Sutton, A. J., Takahashi, T., Tilbrook, B., van der Werf, G. R., Viovy, N., Wang, Y. P.,
588 Wanninkhof, R., Wiltshire, A., and Zeng, N.: Global carbon budget 2014, *Earth System Science Data*, 7, 47-85,
589 10.5194/essd-7-47-2015, 2015.

590 Liss, P. S., and Slater, P. G.: Flux of gases across the air-sea interface, *Nature*, 247, 181-184, 1974.

591 Liss, P. S., and Merlivat, L.: Air-sea gas exchange rates: introduction and synthesis, in: *The role of air-sea*
592 *exchange in geochemical cycling*, edited by: Buatmenard, P., Reidel, 113-127, 1986.

593 Marandino, C. A., de Bruyn, W. J., Miller, S. D., and Saltzman, E. S.: Eddy correlation measurements of the
594 air/sea flux of dimethylsulfide over the North Pacific Ocean, *Journal of Geophysical Research-Atmospheres*, 112,
595 art. no.-D03301, 10.1029/2006jd007293, 2007.

596 McGillis, W. R., Dacey, J. W. H., Frew, N. M., Bock, E. J., and Nelson, R. K.: Water-air flux of dimethylsulfide,
597 *J Geophys Res-Oceans*, 105, 1187-1193, 2000.

598 McGillis, W. R., Edson, J. B., Hare, J. E., and Fairall, C. W.: Direct covariance air-sea CO₂ fluxes, *J Geophys*
599 *Res-Oceans*, 106, 16729-16745, 2001.

600 Melville, W. K., and Matusov, P.: Distribution of breaking waves at the ocean surface, *Nature*, 417, 58-63, 2002.

601 Miller, S. D., Hristov, T. S., Edson, J. B., and Friehe, C. A.: Platform motion effects on measurements of
602 turbulence and air-sea exchange over the open ocean, *Journal of Atmospheric and Oceanic Technology*, 25, 1683-
603 1694, 10.1175/2008jtech0547.1, 2008.

604 Miller, S. D., Marandino, C., de Bruyn, W., and Saltzman, E. S.: Air-sea gas exchange of CO₂ and DMS in the
605 North Atlantic by eddy covariance, *Geophysical Research Letters*, 36, art. no.-L15816, 10.1029/2009gl038907,
606 2009.

607 Miller, S. D., Marandino, C., and Saltzman, E. S.: Ship-based measurement of air-sea CO₂ exchange by eddy
608 covariance, *Journal of Geophysical Research-Atmospheres*, 115, art. no.-D02304, 10.1029/2009jd012193, 2010.

609 Pereira, R., Schneider-Zapp, K., and Upstill-Goddard, R. C.: Surfactant control of gas transfer velocity along an
610 offshore coastal transect: results from a laboratory gas exchange tank, *Biogeosciences*, 13, 3981-3989,
611 10.5194/bg-13-3981-2016, 2016.

612 Rhee, T. S., Nightingale, P. D., Woolf, D. K., Caulliez, G., Bowyer, P., and Andreae, M. O.: Influence of energetic
613 wind and waves on gas transfer in a large wind-wave tunnel facility, *J Geophys Res-Oceans*, 112, art. no.-C05027,
614 10.1029/2005jc003358, 2007.

615 Saltzman, E. S., King, D. B., Holmen, K., and Leck, C.: Experimental determination of the diffusion coefficient
616 of dimethylsulfide in water, *J Geophys Res-Oceans*, 98, 16481-16486, 1993.

617 Saltzman, E. S., de Bruyn, W. J., Lawler, M. J., Marandino, C. A., and McCormick, C. A.: A chemical ionization
618 mass spectrometer for continuous underway shipboard analysis of dimethylsulfide in near-surface seawater,
619 *Ocean Science*, 5, 537-546, 2009.

620 Scanlon, B., and Ward, B.: Oceanic wave breaking coverage separation techniques for active and maturing
621 whitecaps, *Methods in Oceanography*, 8, 1-12, 10.1016/j.mio.2014.03.001, 2013.

622 Schwendeman, M., and Thomson, J.: Observations of whitecap coverage and the relation to wind stress, wave
623 slope, and turbulent dissipation, *Journal of Geophysical Research: Oceans*, 120, 8346-8363,
624 10.1002/2015jc011196, 2015.

625 Stefels, J., Steinke, M., Turner, S., Malin, G., and Belviso, S.: Environmental constraints on the production and
626 removal of the climatically active gas dimethylsulphide (DMS) and implications for ecosystem modelling,
627 *Biogeochem*, 83, 245-275, 10.1007/s10533-007-9091-5, 2007.

628 Virkkula, A., Teinilä, K., Hillamo, R., Kerminen, V.-M., Saarikoski, S., Aurela, M., Koponen, I. K., and Kulmala,
629 M.: Chemical size distributions of boundary layer aerosol over the Atlantic Ocean and at an Antarctic site, *Journal*
630 *of Geophysical Research-Atmospheres*, 111, art. no.-D05306, 10.1029/2004jd004958, 2006.

631 Wanninkhof, R., Ledwell, J. R., and Broecker, W. S.: Gas exchange-wind speed relation measured with sulfur
632 hexafluoride on a lake, *Science*, 227, 1224-1226, 10.1126/science.227.4691.1224, 1985.

633 Wanninkhof, R.: Relationship between wind speed and gas exchange over the ocean, *J Geophys Res-Oceans*, 97,
634 7373-7382, 1992.

635 Wanninkhof, R., and Knox, M.: Chemical enhancement of CO₂ exchange in natural waters, *Limnology and*
636 *Oceanography*, 41, 689-697, 10.4319/lo.1996.41.4.0689, 1996.

637 Watson, A. J., Upstill-Goddard, R. C., and Liss, P. S.: Air-sea gas exchange in rough and stormy seas measured
638 by a dual-tracer technique, *Nature*, 349, 145-147, 1991.

639 Weiss, R. F.: Carbon dioxide in water and seawater: The solubility of a non-ideal gas, *Marine Chemistry*, 2, 203-
640 215, [http://dx.doi.org/10.1016/0304-4203\(74\)90015-2](http://dx.doi.org/10.1016/0304-4203(74)90015-2), 1974.

641 Woolf, D. K.: Bubbles and the air-sea transfer velocity of gases, *Atmosphere-Ocean*, 31, 517-540, 1993.

642 Woolf, D. K.: Bubbles and their role in gas exchange, in: *The Sea Surface and Global Change*, edited by: Liss, P.
643 S., and Duce, R. A., Cambridge University Press, Cambridge, 173-205, 1997.

644 Woolf, D. K.: Parametrization of gas transfer velocities and sea-state-dependent wave breaking, *Tellus Series B-*
645 *Chemical and Physical Meteorology*, 57, 87-94, 2005.

646 Woolf, D. K., Leifer, I. S., Nightingale, P. D., Rhee, T. S., Bowyer, P., Caulliez, G., de Leeuw, G., Larsen, S. E.,
647 Liddicoat, M., Baker, J., and Andreae, M. O.: Modelling of bubble-mediated gas transfer: Fundamental principles
648 and a laboratory test, *Journal of Marine Systems*, 66, 71-91, <http://dx.doi.org/10.1016/j.jmarsys.2006.02.011>,
649 2007.

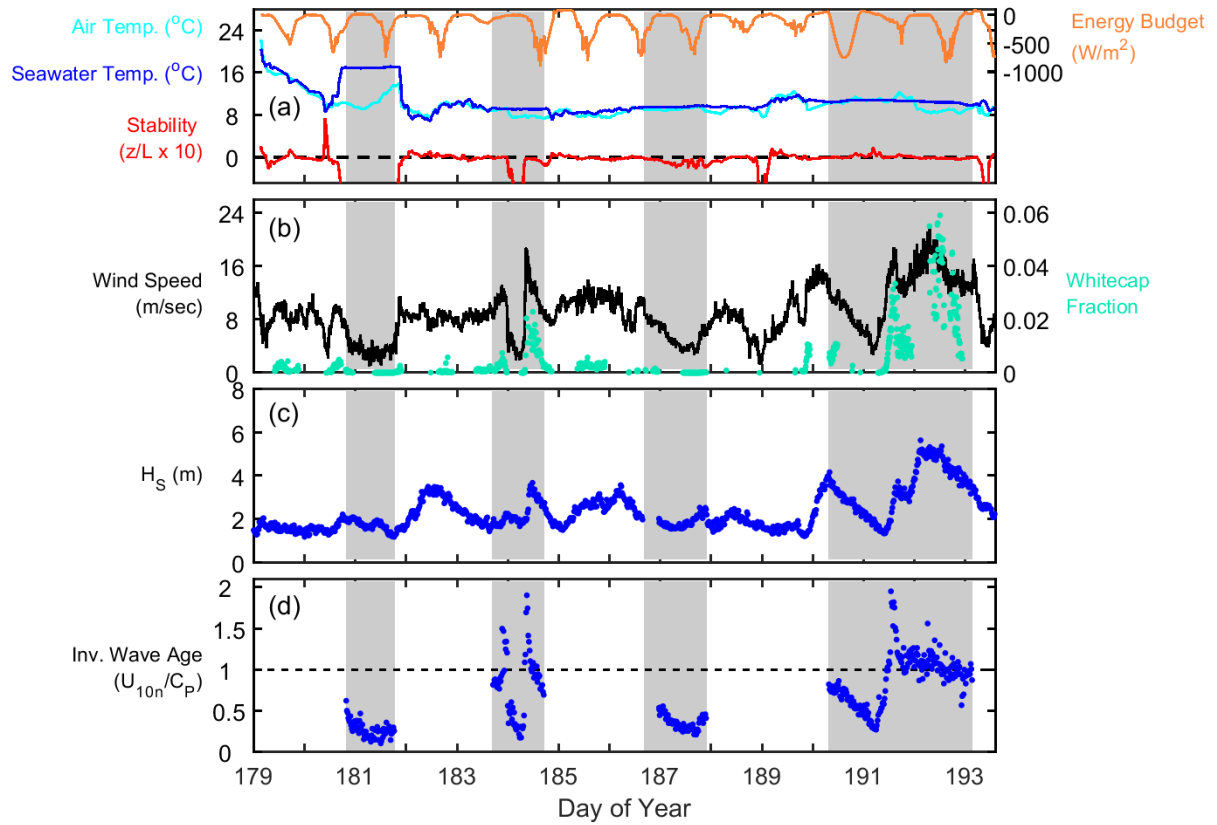
650 Woolf, D. K., Land, P. E., Shutler, J. D., Goddijn-Murphy, L. M., and Donlon, C. J.: On the calculation of air-sea
651 fluxes of CO₂ in the presence of temperature and salinity gradients, *Journal of Geophysical Research: Oceans*,
652 121, 1229-1248, 10.1002/2015jc011427, 2016.

653 Yang, M., Blomquist, B. W., Fairall, C. W., Archer, S. D., and Huebert, B. J.: Air-sea exchange of dimethylsulfide
654 in the Southern Ocean: Measurements from SO GasEx compared to temperate and tropical regions, *J Geophys*
655 *Res-Oceans*, 116, art. no.-C00F05, 10.1029/2010jc006526, 2011.

656 Yang, M., Beale, R., Liss, P., Johnson, M., Blomquist, B., and Nightingale, P.: Air-sea fluxes of oxygenated
657 volatile organic compounds across the Atlantic Ocean, *Atm Chem Phys*, 14, 7499-7517, 10.5194/acp-14-7499-
658 2014, 2014.

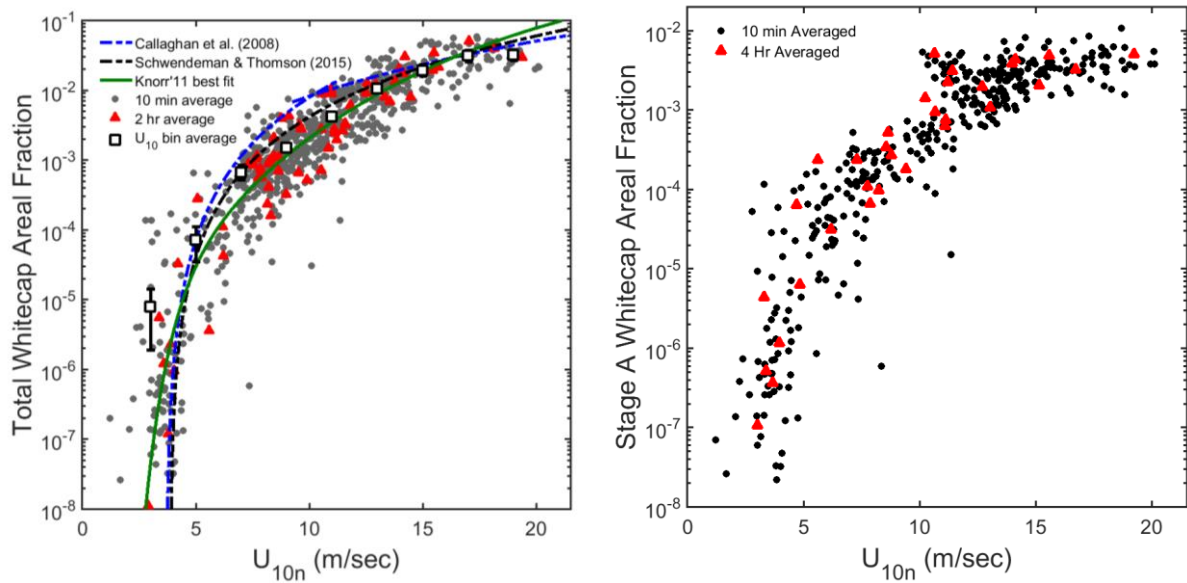
659

660

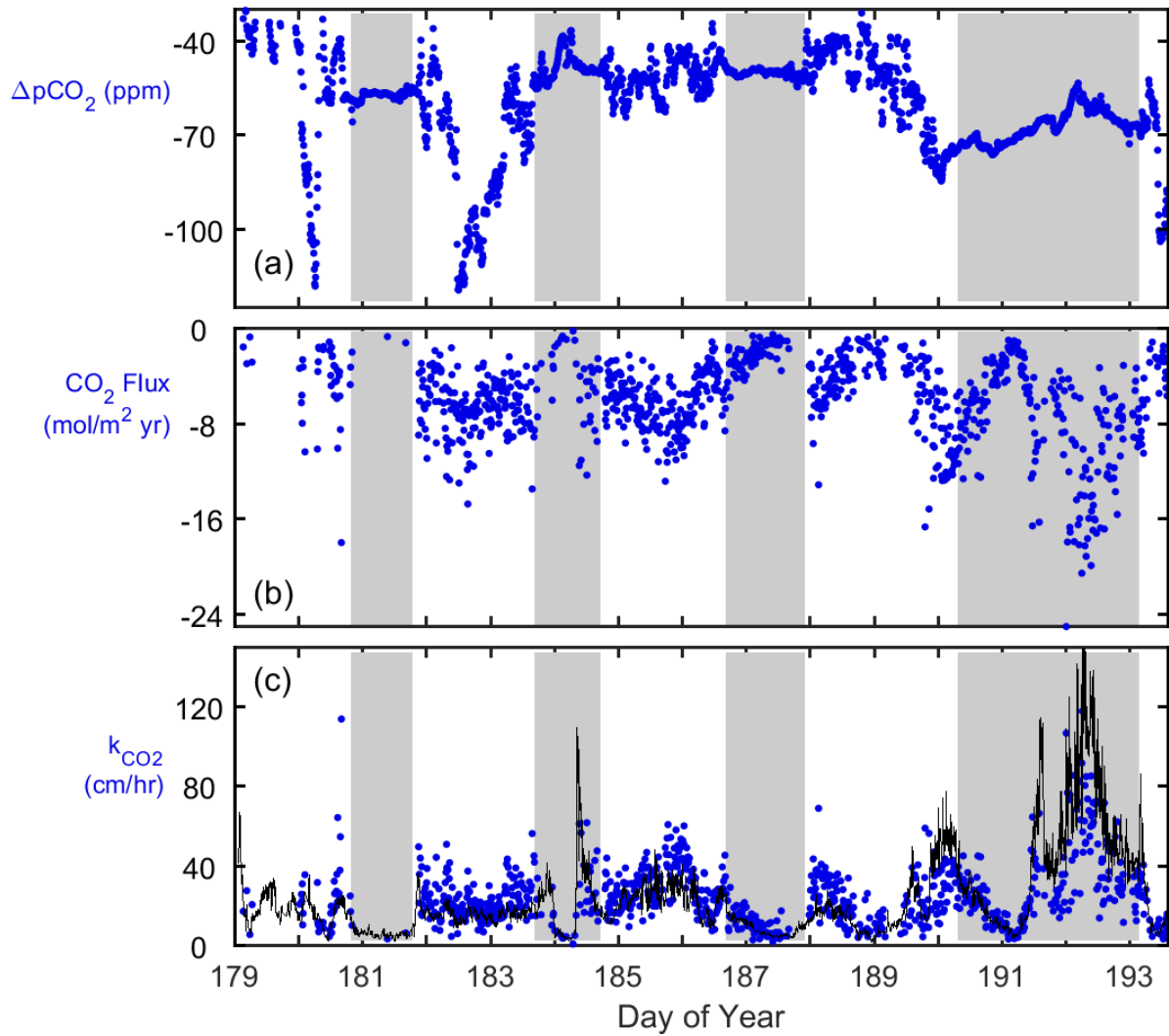


661

662 **Figure 1:** Time series of ten minute averaged data collected during the Knorr_11 cruise. Dashed black
 663 line in panel (a) indicates neutral atmospheric stability ($z/L = 0$). Grey shaded regions represent
 664 intervals when the ship occupied stations ST181, ST184, ST187, and ST191. Measured wave properties
 665 (see Bell et al., 2013) are presented in panel (c) and (d): significant wave height (H_s , c) and inverse
 666 wave age (d). $U_{10n}/C_p \geq 1$ represent younger seas and $U_{10n}/C_p < 1$ represent older seas.
 667



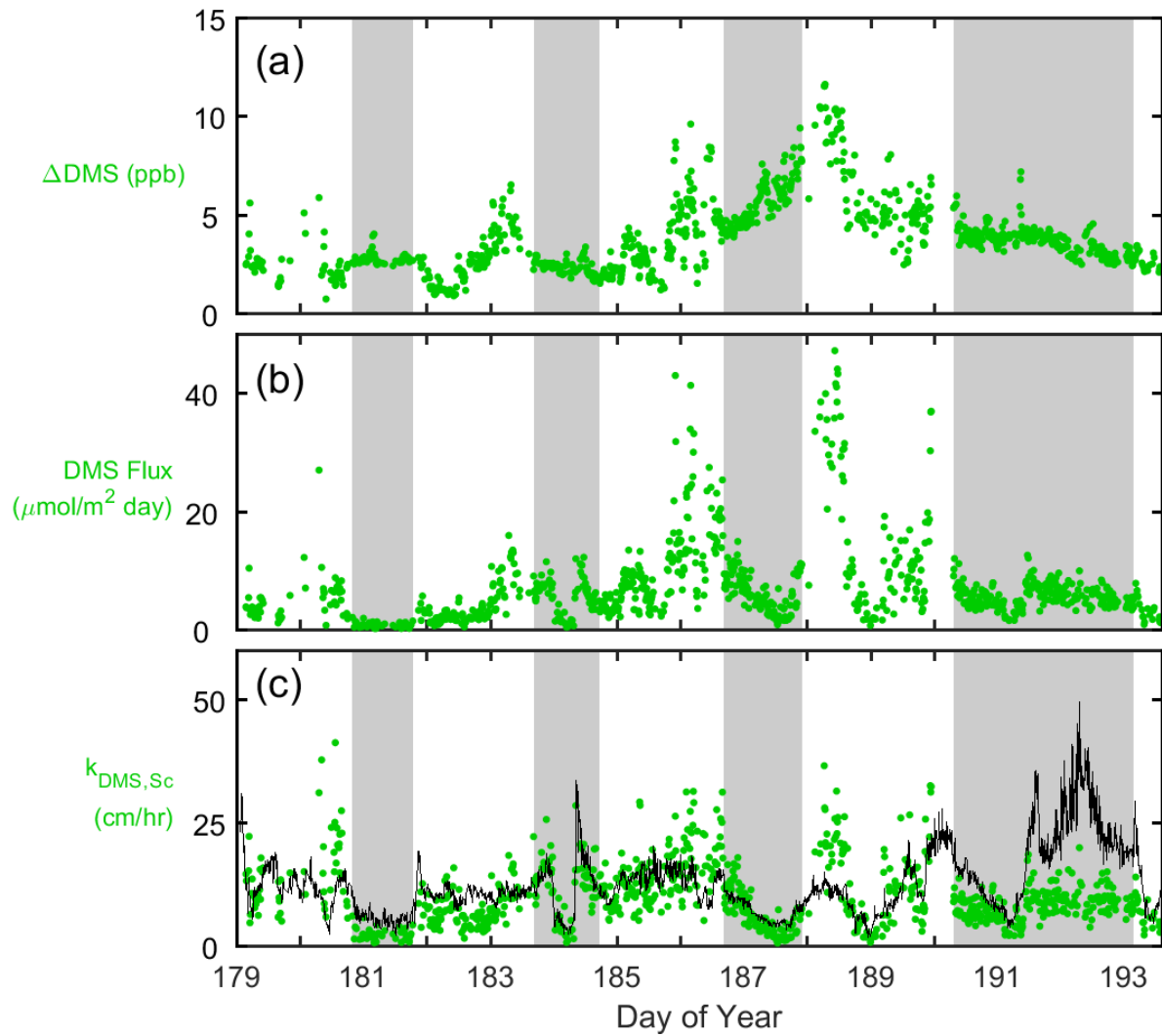
670 **Figure 2:** Semi-log plots of whitecap areal fraction as a function of mean horizontal wind speed at 10
 671 m above the sea surface (U_{10n}) during the Knorr_11 cruise. 10 min average (grey dots) and 2 hour
 672 average (red triangles) data are shown on both panels. Left panel shows total whitecap area (W_T) versus
 673 U_{10n} bin averaged data (open squares, 2 m s^{-1} bins). The best fit line to Knorr'11 2 hr average data
 674 (green; $\log_{10}(W_T) = -42.19e^{(-0.95U)} - 6.5e^{(-0.0886U)}$) and wind speed parameterisations from the recent
 675 literature are shown for reference. Right panel is the whitecap area considered to be solely from wave
 676 breaking (Stage A whitecaps (W_A), see text for definition).
 677



678

679 **Figure 3:** Knorr_11 cruise time series of ten minute averaged CO_2 : (a) air/sea concentration difference
 680 ($\Delta p\text{CO}_2$); (b) flux (F_{CO_2}); and (c) gas transfer velocity (k_{CO_2}) (water-side only, no Sc correction). Panel
 681 (c) also shows k_{CO_2} calculated using the NOAA COARE model (black line). Note that negative k_{CO_2}
 682 data points in (c) were omitted for clarity (see Supplemental Figure S6 for full data set). Grey shaded
 683 regions represent periods on station.

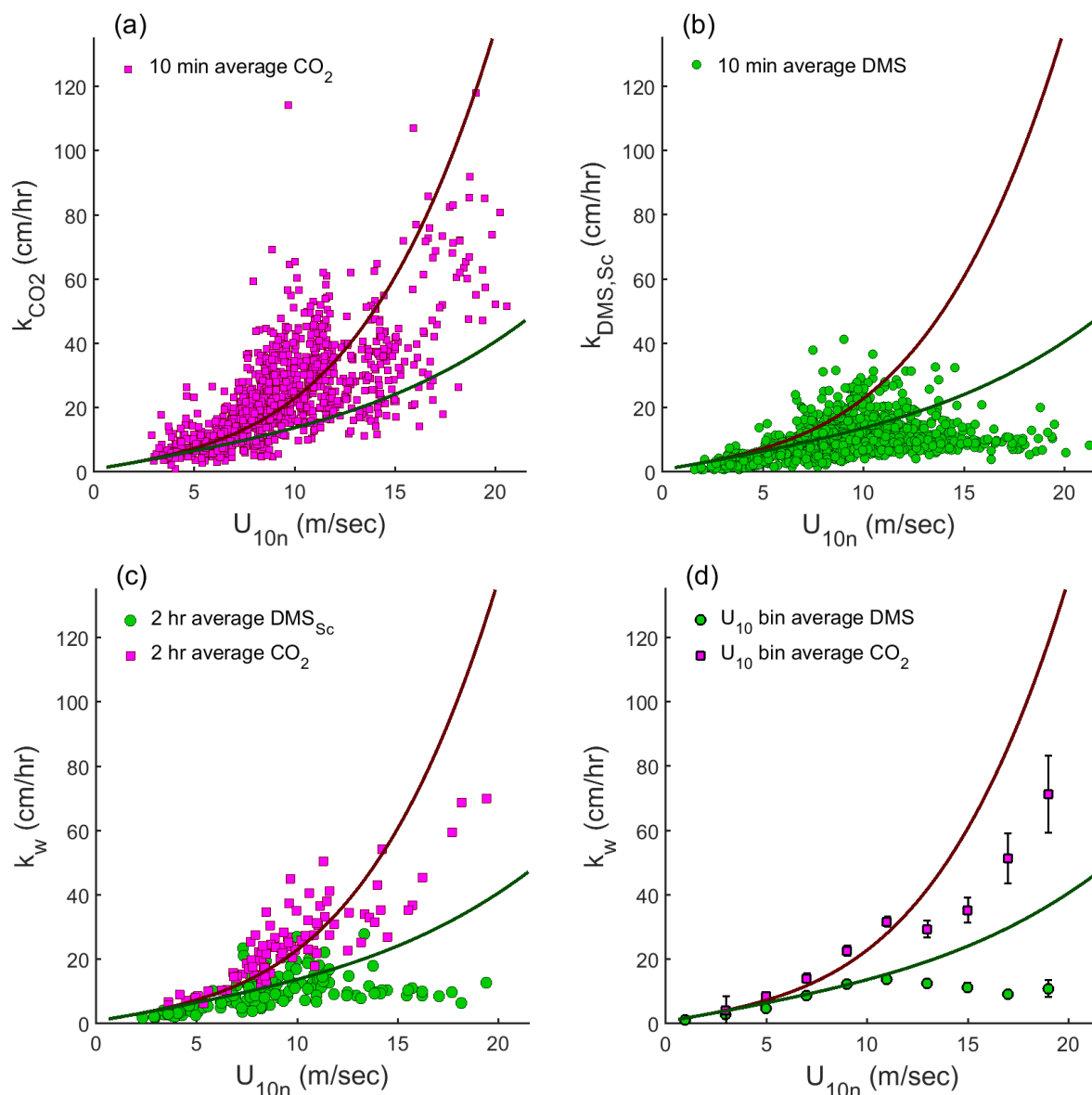
684



685

686 **Figure 4:** Knorr_11 cruise time series of ten minute averaged DMS: (a) air/sea concentration difference
 687 (ΔDMS); (b) flux (F_{DMS}); and (c) gas transfer velocity normalised to the *in situ* CO_2 Sc number ($k_{\text{DMS},Sc}$).
 688 Panel (c) shows $k_{\text{DMS},Sc}$ calculated using NOAA COARE model output (black line). Grey shaded regions
 689 represent periods on station.
 690

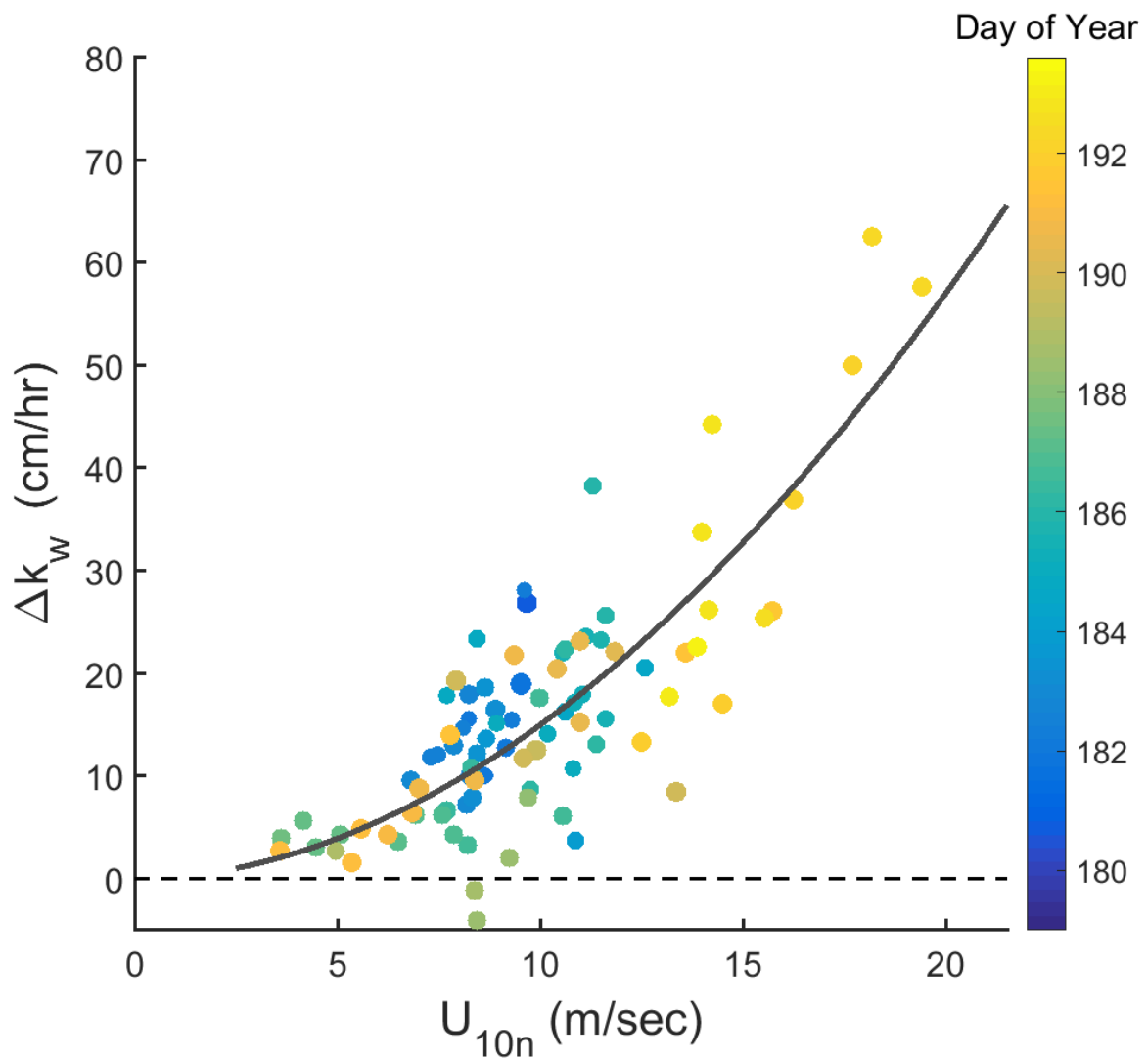
691



692

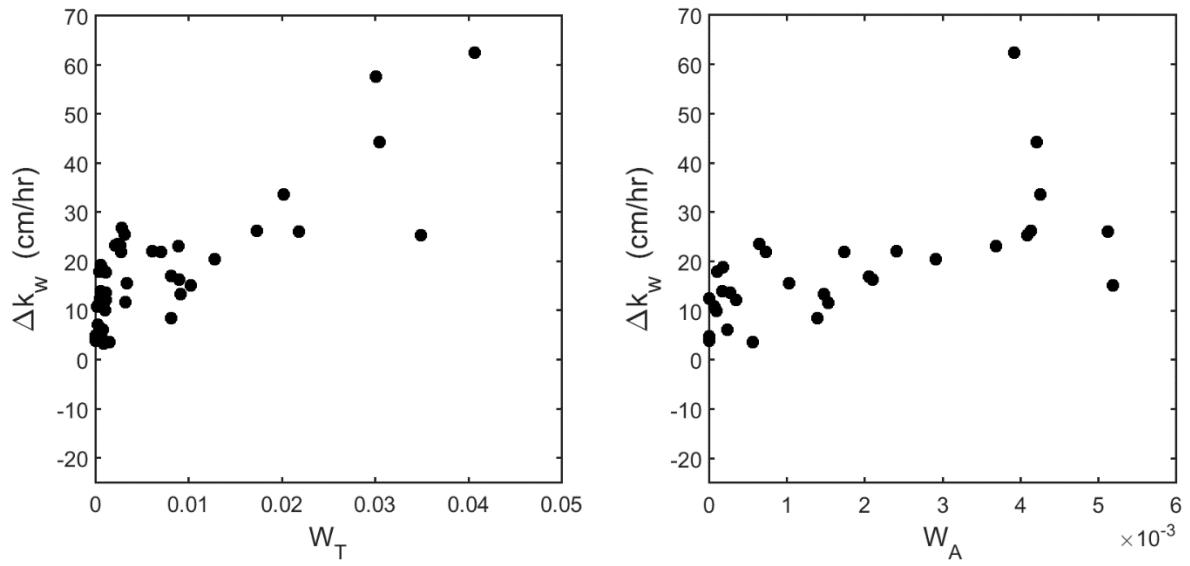
693

694 **Figure 5:** Gas transfer velocities plotted against mean horizontal wind speed (U_{10}) from the Knorr_11
 695 cruise. Ten minute average data for CO_2 (a) and DMS (b). DMS gas transfer velocities are normalised
 696 to the *in situ* CO_2 Sc number. Data are averaged into 2 hour periods (c) and 2 m s^{-1} wind speed bins (d).
 697 Note that negative k_{CO_2} data in (a) have not been plotted for clarity (see Supplemental Figure S8 for full
 698 data set). For reference, the NOAA COAREG3.1 model output for CO_2 (magenta line) and DMS (green
 699 line) is plotted on all four panels. The COARE model was run with the turbulent/molecular coefficient,
 700 $A = 1.6$, and the bubble-mediated coefficient, $B = 1.8$, and used mean Knorr_11 data for the input
 701 parameters.
 702



703

704 **Figure 6:** Difference (Δk_w) between 2 hour average k_{CO_2} and $k_{DMS,Sc}$ plotted against U_{10} . Data are
 705 coloured by the date of measurement (Day of Year). The solid grey line describes the power law fit to
 706 the data (see Equation 7).
 707



708

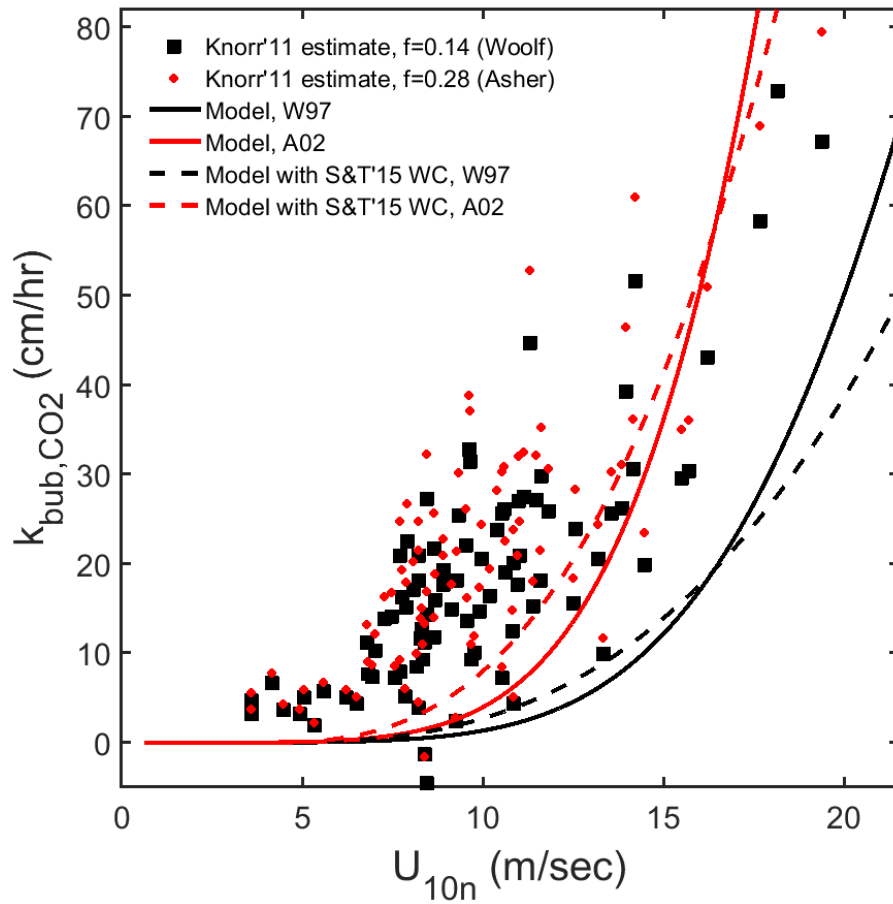
709

710

711

712

Figure 7: Knorr_11 Δk_w data plotted against total whitecap areal fraction (left panel) and against Stage A whitecap areal fraction (right panel). Each point is a 2 hour average of coincident measurements of whitecap fraction and DMS and CO_2 gas transfer.



713

714 **Figure 8:** Bubble-mediated transfer velocity of CO₂ (k_{bub,CO_2}) as a function of wind speed. Individual
 715 points are Knorr_11 observations using solubility and diffusivity scaling from Woolf (1997) (black
 716 squares) and Asher et al. (2002) (red circles). Continuous lines are model calculations of k_{bub,CO_2} using
 717 the Knorr_11 wind speed-whitecap areal fraction relationship (see Figure 2) and mean SST (Woolf
 718 (1997), black; Asher et al. (2002), red). Model calculations were also performed using the
 719 Schwendeman and Thomson (2015) wind speed-whitecap areal fraction relationship (dashed lines).

720